energies

MDPI

Article

Thermal Cycling in Converter IGBT Modules with Different Cooling Systems in Pitch- and Active Stall-Controlled Tidal Turbines

Faisal Wani [1,*,†], Udai Shipurkar [2], Jianning Dong [3] and Henk Polinder [4]

[1] Huygens Engineers, 2516 AH The Hague, The Netherlands
[2] Ships, Maritime Research Institute Netherlands (MARIN), 6708 PM Wageningen, The Netherlands; U.Shipurkar@marin.nl
[3] Electrical Sustainable Energy, Delft University of Technology, 2628 CD Delft, The Netherlands; J.Dong-4@tudelft.nl
[4] Maritime and Transportation Technology, Delft University of Technology, 2628 CD Delft, The Netherlands; H.Polinder@tudelft.nl
* Correspondence: f.wani@huygens-engineers.nl; Tel.: +31-85-0802801
† Current address: Mekelweg 2, 2628 CD Delft, The Netherlands.

Abstract: This paper compares active and passive cooling systems in tidal turbine power electronic converters. The comparison is based on the lifetime of the IGBT (insulated gate bipolar transistor) power modules, calculated from the accumulated fatigue due to thermal cycling. The lifetime analysis accounts for the influence of site conditions, namely turbulence and surface waves. Results indicate that active cooling results in a significant improvement in IGBT lifetime over passive cooling. However, since passive cooling systems are inherently more reliable than active systems, passive systems can present a better solution overall, provided adequate lifetime values are achieved. On another note, the influence of pitch control and active speed stall control on the IGBT lifetime was also investigated. It is shown that the IGBT modules in pitch-controlled turbines are likely to have longer lifetimes than their counterparts in active stall-controlled turbines for the same power rating. Overall, it is demonstrated that passive cooling systems can provide adequate cooling in tidal turbine converters to last longer than the typical lifetime of tidal turbines (>25 years), both for pitch-controlled and active speed stall-controlled turbines.

Keywords: forced water cooling; insulated gate bipolar transistors; lifetime estimation; passive cooling; reliability; submerged power electronic converter; thermal cycling; tidal turbines; turbulence; waves

Citation: Wani, F.; Shipurkar, U.; Dong, J.; Polinder, H. Thermal Cycling in Converter IGBT Modules with Different Cooling Systems in Pitch- and Active Stall-Controlled Tidal Turbines. *Energies* **2021**, *14*, 6457. https://doi.org/10.3390/en14206457

Academic Editor: Ui-Min Choi

Received: 10 July 2021
Accepted: 16 September 2021
Published: 9 October 2021

1. Introduction

Tidal energy is a predictable source of energy, which gives it an advantage over other renewable forms of energy. Among methods of harvesting tidal energy, tidal stream turbines (TSTs) are becoming popular compared to tidal dams. Currently, however, the cost of energy from TSTs is high compared to traditional forms of clean energy [1]. To minimize the cost of energy, improving reliability and/or minimizing maintenance expenses is necessary [1]. In this regard, this paper investigates the reliability of power electronic converters in different TST energy conversion systems. The TST systems in this paper are classified based on the cooling system in the power electronic converters (passive and forced-water cooling) and the power regulation scheme employed in the turbine (pitch and stall control).

A typical tidal stream turbine system is shown in Figure 1. For array instalments, a submerged converter is more suitable than onshore converters; this makes converter reliability even more critical [2]. Power converters require cooling in order to prevent their early failure from thermo-mechanical stress. Such failures occur mostly in IGBT (insulated

gate bipolar transistors) power modules from thermal cycling [3,4]. The time to failure from this failure mechanism can be prolonged by providing adequate cooling to the IGBT power modules. For a submerged power converter, an active cooling method, such as forced-water cooling, is undesirable due to the limited opportunities for maintenance [5]. On the other hand, passive cooling systems offer a higher degree of reliability, albeit at a lower cooling efficacy [3,5]. Therefore, a comparison between different cooling systems becomes imperative.

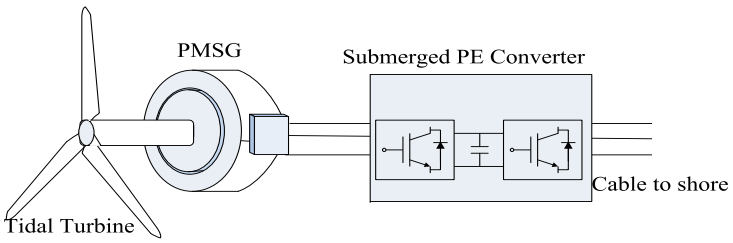

Figure 1. Tidal turbine drive train with a direct-drive permanent magnet synchronous generator (PMSG) and a power electronic (PE) converter [2].

In a passively cooled system, IGBT modules can be mounted directly on the interior walls of the sealed enclosure via a mounting plate, as shown in Figure 2 [5,6]. The external walls of the enclosure directly exchange heat with the seawater via natural convection. For actively cooled systems, the modules are mounted on a heat sink through which a coolant is driven by means of a pump [3], as seen in Figure 3.

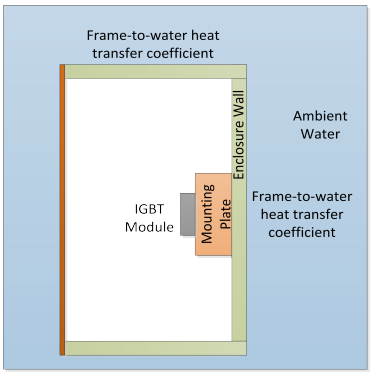

Figure 2. Passive cooling: IGBT module in a submerged and hermetically sealed power converter [5].

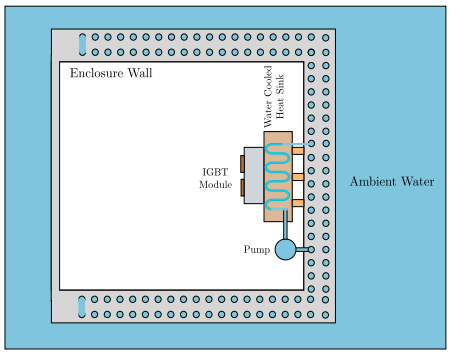

Figure 3. Active cooling: Water is passed through a heat sink on which the IGBT modules are mounted. The coolant then exchanges the heat with the ambient seawater through a separate heat exchanger, which may be embedded in the enclosure walls. This is only a representative diagram; heat exchangers on the cabinet surface can look differently than presented here.

This paper furthers the work done in [2], where the lifetime analysis of IGBT modules in a passively cooled converter was studied. In this paper, the feasibility of the passive cooling system is evaluated by comparing it with an active cooling system. Here, by active cooling system, a forced-water cooling system is implied. The reason is that forced-water cooling is the standard choice in tidal turbine converters, whereas passive cooling offers higher reliability, is cheaper, and involves no energy consumption. The cooling systems are compared in terms of the mean junction temperatures, the amplitude of thermal cycling, annual losses in the IGBT modules, and damage distribution with respect to the tidal velocity. We also overrate the forced-water cooling system to show how it can be used to further improve the lifetime.

Furthermore, the lifetime of the IGBT modules is evaluated in two similarly rated (power and speed) tidal turbines. The turbines differ in the mechanism of power regulation beyond the rated speed. One of the turbines utilizes active speed stall control, whereas the other employs pitch control [7,8]. Both these systems can be found in commercial tidal turbines [9].

The main contributions from this paper can be summarized as:

- Evaluating active and passive cooling systems in terms of the lifetime of IGBT modules in tidal turbine converters;
- Studying the impact of active speed stall and pitch control on the IGBT lifetime.

To the best of our knowledge, these factors have not been addressed in the literature before for the TST applications. The paper does not claim any novelty in terms of methodology or measurement techniques. The contribution is primarily presenting trade-offs in the selection of power electronic converter rating and topology from the viewpoint of improving the reliability of TST systems.

The rest of the paper is structured as follows. The following section gives a literature review of active and passive cooling systems used for the cooling of power semiconductor devices (including IGBT modules) and lifetime analyses of IGBT modules. In doing so, Section 2 also justifies the system selected for this study. In Section 3, the description of the tidal stream turbine system used for analysis in this paper is given. Section 4 describes the methodology adopted for the calculation of IGBT module lifetime. Section 5 briefly explains the thermal model for active (forced-water) and passive cooling systems. Section 6 gives the results for the IGBT lifetimes for active and passive cooling systems on two 110 kW tidal turbine systems (active speed stall- and pitch-controlled turbines). Conclusions from the paper are given in Section 7.

2. Literature Review

Few data are available regarding the failures of power electronics in tidal turbines. Due to the similarity with wind turbines, it is reasonable to assume that similar failures would occur in TSTs. For direct drive generators with fully rated converters, a majority of the converter failures relate to the cooling system [10–12].

IGBT modules are one of the most commonly failing components in power converters [13–15]. Multiple studies suggest that IGBT modules fail due to fatigue accumulated from thermal cycling [15–17]. Such failures are mainly due to ageing of bond-wires [16,18] and solder fatigue [16,19].

However, recently, Fischer et al. [14] claimed that most failures in wind turbines occurred from moisture and humidity, rather than thermal cycling. Because the submerged converter is hermetically sealed, the moisture amount in the enclosure can be controlled. No fresh air circulates in the cabinet, and the moisture already present inside can be absorbed by materials, such as silica. Another alternative could be to fill the cabinet with dehumidified air before submersion. Under these circumstances, thermal cycling can be expected to be a major failure mode in subsea power electronics.

The cooling methods for IGBTs can broadly be classified into active and passive cooling methods. Active methods are comprised of [3]:

- Forced-air cooling;

- Forced-liquid cooling;
- Micro-channel heat sinks;
- Two-phase forced convection cooling;
- Jet impingement and spray cooling;
- Hybrid solid and liquid cooling.

Active cooling systems can also be adaptively controlled to improve the lifetime of IGBT modules [20,21] by controlling the sink-to-ambient thermal resistance. Most actively cooled systems utilize rotating components, such as pumps, which compromise reliability. However, an exception can be found in [22], where a liquid metal coolant is driven by a magnetohydrodynamic pump. However, this system comes with its own set of challenges and is not examined here.

On the other hand, passive cooling could be either of the following:

- Air cooling [3];
- Submerged water cooling [5,6].

Of these aforementioned cooling techniques, this paper compares forced-liquid (water) cooling with submerged water cooling. This is because these two systems are more likely to be found in submerged TST power converters.

In addition to cooling, the lifetime of converters can also be enhanced by using different converter topologies [15,23] in three-level converters. This paper, however, focuses on a two-level back-to-back converter. Two-level converters are widely used for low voltage applications owing to their simplicity [24]. Other methods of improving lifetime include control of modulation strategies, switching frequency, reactive current circulation, active gate gate-driver control, and, in the case of parallel converters, power loss redistribution [25–31]. These methods are not investigated in this paper, and the focus is solely on cooling system.

Ma and Blaabjerg [32] compared thermal performance in a three-level NPC converter with IGBT module, IGBT press-pack, and IGCT press-pack packaging technologies. IGBT modules were shown to have the lowest losses and lowest temperature cycling compared to the other two technologies. Furthermore, IGBT modules exhibit better insulation between the chip and heat sink and are cheaper and easier to maintain [4,32]. For these reasons, IGBT modules are more prevalent in renewable energy applications and are thus analysed in this paper.

Lifetime estimation during the design phase is a critical step in ensuring long term reliability [33]. Lifetime evaluation of IGBT modules mostly falls under either a priori lifetime assessment or condition monitoring techniques [13,18]. The former requires prior knowledge of loading patterns and system parameters and is mainly done for an estimate of lifetime prior to deployment. The latter is more concerned with real-time measurements and monitoring ageing in the modules. This paper deals with the lifetime assessment prior to deployment.

The aforementioned literature addresses several aspects related to the lifetime analysis of power semiconductor devices. However, none of the research has analysed IGBT lifetimes either in the context of comparing passive and active cooling systems or in the context of active speed stall and pitch control in submerged TSTs. Furthermore, assuming a passive cooling system is inherently more reliable than an active cooled one, the objective is to study the feasibility of the passive system over the active one. This paper addresses these questions by means of investigating a TST system described in the following section.

3. System Description

The lifetime of IGBT modules depends strongly on their loading mission profile as well as the system design [2,27]. Thus, defining the site conditions and the turbine-generator-converter specifications is mandatory to contextualize the obtained lifetime results.

3.1. Site Conditions

The main characteristics of a tidal site pertinent for lifetime analysis are the mean tidal velocity, turbulence in the tidal stream velocity, and surface waves [2]. The parameters used in this paper are the same as those used in [2].

The main idea behind defining these parameters is to obtain a realistic instantaneous tidal stream velocity time series. This is achieved by the superimposition of turbulence and surface wave induced oscillations on the mean tidal stream velocity, as described in [2]:

$$v_{tide}(t) = v_{mean} + \Delta v_{turbulence} + \Delta v_{waves} \ . \tag{1}$$

These components are described in Appendix A. For a more detailed understanding of how v_{mean}, $\Delta v_{turbulence}$, and Δv_{waves} are used in calculating the time series of the tidal stream velocity, please see [2,34]. Please note that this study only accounts for the ambient turbulence. Turbulence induced due to stall operation or pitch control at the blades is not included in this study. These effects might have a further impact on the lifetime and must be considered in a future study.

An example of a tidal stream velocity time series is shown in Figure 4. The necessary turbine parameters are listed in Table 1.

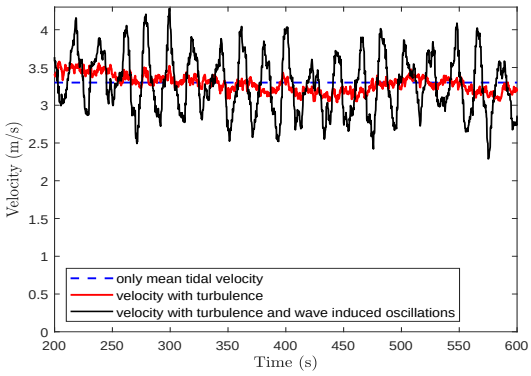

Figure 4. Fluctuations in the tidal stream velocity about its mean value (here taken as 3.3 m/s) as a consequence of turbulence and wave induced oscillations are shown here. In this figure, a TI value of 13% is used, and a surface wave of significant wave height Hs = 5.75 m and peak period = 11 s are used. This is an extreme case of wave induced oscillation to highlight the impact of waves. It must be noted such waves rarely occur [2].

Table 1. Turbine rotor parameters.

Parameter	Value
Rotor diameter	6.5 m
Rated tidal stream speed	2.5 m/s
Hub depth from surface	20 m
Seabed depth from surface	30 m

3.2. Turbine and Generator Specifications

Our previous work [2] performed a lifetime analysis of a fixed-pitch turbine rated at 110 kW with a rated speed of 30 rpm. Power regulation of the fixed-pitch turbine was achieved by the active speed stall mechanism. In this paper, the fixed-pitch turbine is compared with a pitch-controlled turbine [2,7,8]. For comparison purposes, both turbines are rated at 110 kW and have the same power-tidal speed curve shown in Figure 5. However, their rpm-tidal speed profiles are different, as shown in Figure 6. The maximum value of C_p for both the turbines is roughly 0.43, and thus they have the same power output even below the rated tidal stream speed.

The active speed stall-controlled turbine has the following $C_p - \lambda$ equation [2]:

$$C_p(\lambda) = 0.000342\lambda^4 - 0.008056\lambda^3 + 0.046882\lambda^2 - 0.000434\lambda + 0.045225 \quad (2)$$

where C_p is the power coefficient of the turbine, and λ is the tip-speed ratio. Tip-speed ratio is the ratio of the blade tip-speed to the incoming velocity of the fluid.
The pitch-controlled turbine has the following $C_p - \lambda$ relation:

$$C_p(\lambda, \beta) = 0.6\left(\frac{38}{\lambda_1} - 0.25\beta - 2\right) e^{\frac{-11}{\lambda_1}}$$
$$\frac{1}{\lambda_1} = \frac{1}{\lambda + 0.08\beta} - \frac{0.035}{\beta^3 + 1}, \quad (3)$$

where β is the blade pitch angle. The $C_p - \lambda$ curve for the pitch-controlled turbine and the pitch controller used here is similar to that of the 120 kW turbine studied in [35]. The maximum rate for the pitch controller is limited to $\pm 5^\circ$ per second.

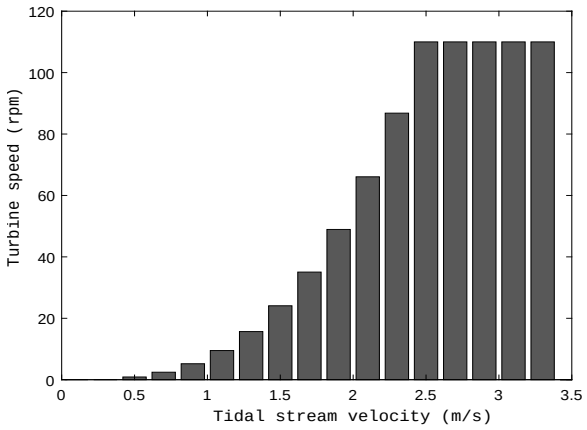

Figure 5. Power curve of the pitch- and active speed (stall)- [2] controlled tidal turbines as a function of tidal stream velocity.

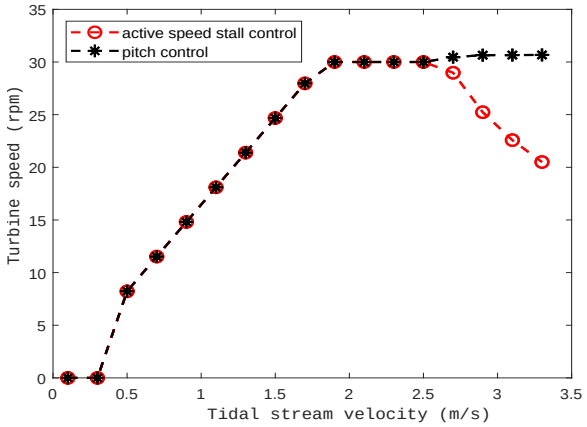

Figure 6. Speed curves of the pitch- and active speed (stall)- [2] controlled tidal turbines as a function of the tidal stream velocity.

For both turbines, the same generator is assumed, which is a direct-drive permanent magnet synchronous generator (PMSG). The parameters of this PMSG are listed in Table 2.

Table 2. Generator parameters.

Parameter	Value
Rated power	110 kW
Rated speed	30 rpm
Pole pairs	40
No-load emf at 30 rpm	188 V
Resistance per phase	0.04 Ω
Synchronous inductance per phase	4 mH
Mass moment of inertia	6100 kg·m^2

Both turbines operate in the maximum power point tracking (MPPT) mode until they reach their rated speed. In the MPPT region, the required torque is given by

$$T^* = K\omega_r^2, \tag{4}$$

where K is a constant depending on factors such as nominal turbine speed and power, maximum value of power coefficient C_p, and the optimal tip-speed ratio, etc. [36]. ω_r is the rotational speed of the turbine. Torque control is achieved by employing the classical PI control strategy in generator dq-axes. The q-axis current is obtained from the desired torque requirement of the generator [2]. If possible, d-axis current is kept at zero. Otherwise, a flux weakening strategy is employed to ensure that the required output voltage is deliverable from the converter [2,37].

Beyond rated speed, the pitch-controlled turbine keeps operating at the rated rpm, using the blade pitch angle to maintain the rated power [35]. On the other hand, in the stall-controlled turbine, the speed of the turbine is reduced to lower C_p and regulate the output power [2].

3.3. Converter Specifications

For the power rating and the voltage level used in this study, a two-level low voltage back-to-back converter is suitable. A representative diagram of this converter is shown in Figure 7. The specifications of interest in the converter are the power loss and thermal parameters of the IGBT modules and the thermal parameters of the cooling system. In this section the specifications for the IGBT modules are given; cooling system specifications are given later in Section 5.

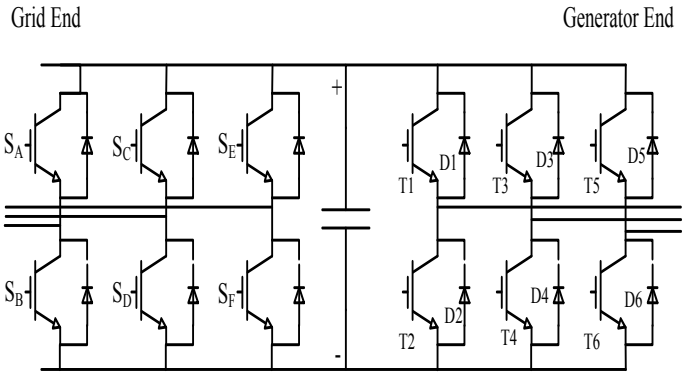

Figure 7. A representative diagram of a two-level voltage source converter [2].

The loss parameters can be determined from the IGBT module datasheet. It is clear that the current rating of the IGBTs in the active stall-controlled must be higher, owing to its lower rpm at rated power. For comparison purposes, the same IGBT module in the pitch-controlled turbine as in the active stall-controlled one is used. The selection of the proper IGBT module for the active stall-controlled turbine is explained in our previous work [2]. For this analysis, Infineon's IGBT module FF600R12ME4 (1200 V, 600 A) is an appropriate choice. The parameters corresponding to this module are listed in Table 3.

Table 3. Converter parameters.

Parameter	**Value**
DC-link voltage	600 V
Switching frequency	2 kHz
DC-link capacitance	102 mF
IGBT part number	**FF600R12ME4**
Voltage and current rating (rms)	1200 V, 600 A
Module dimensions	0.057 m × 0.110 m
IGBT thermal resistance $R_{th,j-c}$ (4-layer Foster form)	[0.0038 0.0312 0.0001 0.0020] K/W
IGBT thermal time constant τ_{th} (4-layer Foster form)	[0.0007 0.0247 0.050 3.485] s
Diode thermal resistance $R_{th,j-c}$ (4-layer Foster form)	[0.0008 0.0489 0.002 0.0057] K/W
Diode thermal time constant τ_{th} (4-layer Foster form)	[0.0006 0.0245 0.0733 0.9951] s

4. Methodology

This section briefly describes how the lifetime of the IGBT module can be estimated based on thermal cycling. The approach used here has been adopted in various studies across applications [15,38–42].

The procedure can be broadly divided into three modelling layers:

1. Estimation of power loss in IGBT modules;
2. Thermal modelling of the IGBT modules;
3. Lifetime estimation based on thermal cycling.

4.1. Estimation of Power Loss

For this purpose, first the converter currents must be determined. This is done using the information about the tidal stream velocity time series, turbine characteristics, and generator and converter parameters, as described in [2,15]. The algorithm is summarised in Figure 8 [2].

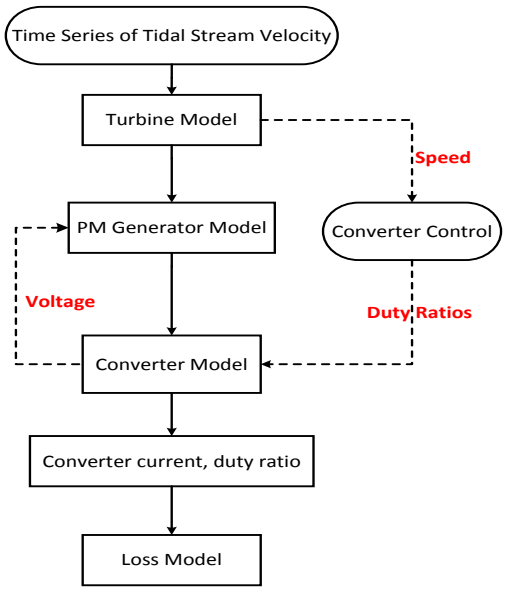

Figure 8. Calculating converter currents and duty ratios for loss calculation in IGBT modules; image adapted from [2].

IGBTs and diodes in a power module experience conduction and switching losses [15,27]. Both of these losses are a function of the junction temperature [43]. Figure 9 shows the

loss calculation flowchart. More details on the loss calculation can be found in multiple references [15,44,45].

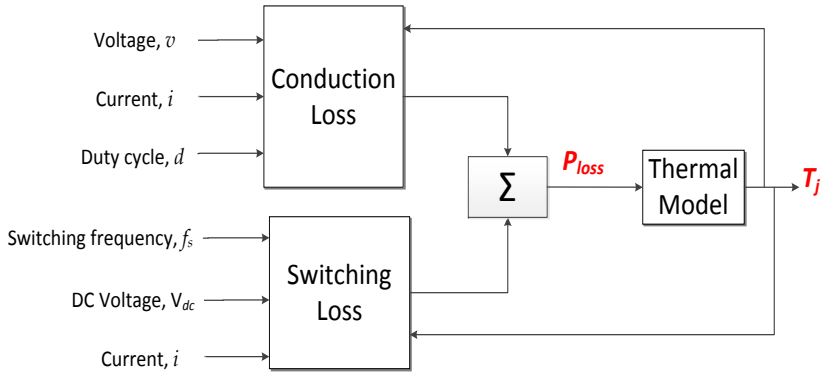

Figure 9. Loss calculation in IGBT and diode. The diagram shows that losses also depend on the junction temperature T_j; hence, the feedback loop from the thermal model.

4.2. IGBT Thermal Modelling

From the power loss in the IGBT modules, thermal models are used to estimate the junction temperature (mean and amplitude). Thermal modelling must be performed for each operating point corresponding to Figure 5, in conjunction with the knowledge of turbulence and surface waves.

Thermal models for IGBT modules can be categorized into three types, namely analytical, numerical, and thermal network models [3]. Analytical models are primarily based on analytical solutions of the heat diffusion equation. These models are fast but can only be applied for simple geometries and with simplified boundary conditions [46,47]. Numerical models are usually based on finite element analysis, sometimes coupled with computational fluid dynamics (CFD) analysis [48,49]. These models are extremely time consuming and are unsuitable for dynamic electro-thermal simulations.

When it comes to using thermal models for lifetime analysis, thermal network models based on RC elements are the most suitable way forward [2,50–52]. The simplicity of these models, fast results, and the possibility of combining RC elements of different individual components (especially in the Cauer form) into a combined RC network of the whole system are their main advantages [51,52]; this is described in Section 5. A main drawback of the simplified one-dimensional RC network models is that the thermal cross-coupling between different IGBT chips within the same module are neglected [4,53]. This may result in an error in junction temperature estimation. However, this error is more likely to contribute to mean junction temperature rather than amplitude of temperature cycling. In other words, such an approximation has little consequence for the final conclusions of this paper.

4.3. Lifetime Estimation

After knowing the junction temperature values, the thermal fatigue accumulated for each operating point is calculated. This is done using the lifetime models for the IGBT power modules as explained below.

The lifetime estimation technique used in this paper is the same as adopted in [2,15]. The number of cycles to failure N_f is estimated based on the models presented in [15,54], given by the equation

$$N_f = A \cdot \Delta T_j^{\beta_1} \cdot e^{\frac{\beta_2}{T_{j,m}+273}} \cdot t_{on}^{\beta_3} \cdot I^{\beta_4} \cdot V^{\beta_5} \cdot D^{\beta_6}. \quad (5)$$

where $T_{j,m}$ is the mean junction temperature, t_{on} is the on-pulse duration, I is the current per wire, V is the chip blocking voltage, and D is the bonding wire diameter. The constants

A and β_1 to β_6 are obtained from [4] and take the following values: $A = 9.34 \times 10^{14}$ for IGBT4 modules, $[\beta_1, \ldots, \beta_6] = [-4.416, 1.285 \times 10^3, -0.463, -0.716, -0.761, -0.5]$.

For each operating point in Figure 5, different values of $N_{f,i}$ and n_i are calculated using the rainflow counting algorithms. Here, n_i is the number of cycles experienced annually, and $N_{f,i}$ is the number of cycles to failure for ith operating point. Subsequently, the net accumulated damage corresponding to all the operating point within a year is estimated from the Miner's rule [38]:

$$Annual \;\; Damage = \sum_i \frac{n_i}{N_f, i} \tag{6}$$

The number of cycles for each thermal cycling amplitude is obtained from Equation (5). Figure 10 shows how N_f typically varies with ΔT_j for constant $T_{j,m}$. The number of years to failure or lifetime (in years) is then calculated as

$$Lifetime \;\; (in \; years) = \frac{1}{Annual \;\; Damage} \tag{7}$$

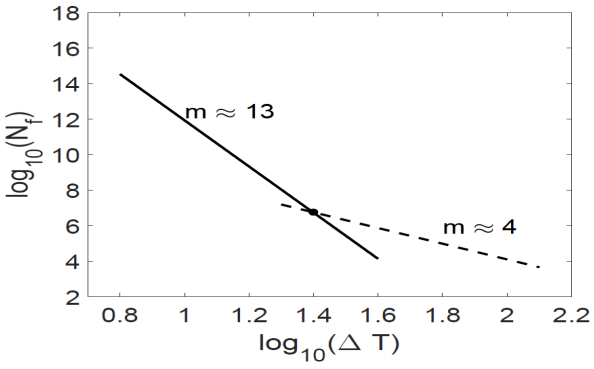

Figure 10. Number of cycles to failure is presented as a function of temperature cycling for a constant mean junction temperature [21].

To take into account the effects of both long term cycling (daily variation in tidal velocity) as well as high frequency cycling due to turbulence and waves, the models are divided into two sections as shown in Figure 11. Multiplying the fatigue for each operating point with the probability of occurrence of each operating point, the net fatigue in the year is calculated. From this information, the number of years to failure is estimated.

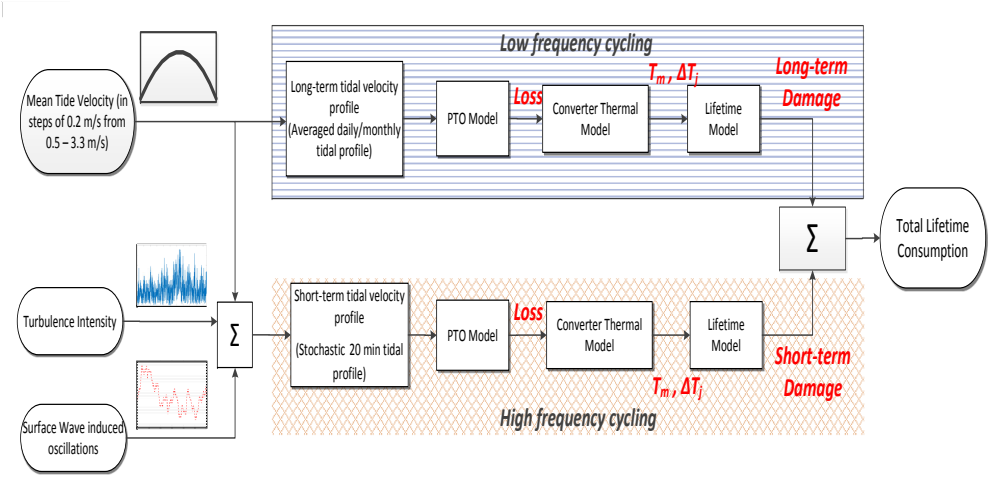

Figure 11. Methodology for lifetime calculations: low and high frequency thermal cycling. Image adapted from [2].

To simplify the calculations, the following assumptions are made.

- The ambient seawater temperature throughout the year is assumed to be 15 °C. This is the maximum temperature at the Orkney (UK) tidal site [55].
- A constant turbulence value has been used for each mean tidal velocity, as described in Appendix A.
- The performance of the turbine is same during the flood and ebb tides [2].
- At the beginning of each flood and ebb tide cycle, the junction temperature of the IGBT module is the same as the ambient temperature.
- Effects of varying reactive power on the thermal cycling of the grid-side converter have been neglected. A constant value (0.9) is assumed [21].

5. Thermal Models for Active and Passive Cooling Systems

In this section a brief explanation is given of how the active (forced-water cooling) and passive cooling systems are modelled into the thermal models for the IGBT modules in a submerged power converter. Furthermore, the specifications of the two cooling systems are also presented, along with necessary assumptions made in the thermal models.

In both active and passive systems, constant thermal resistances (junction-to-case) for the IGBT module are used in this study. In practice, this thermal resistance varies with the temperature [56]. However, when combined with the case-to-ambient thermal resistance, the net variation in junction-to-ambient thermal resistance will not be more than 5% for the extremities observed in this case study. In other words, it is possible that the junction temperature estimation will have an error of 5%. Still, this error is too little to have significant ramifications for the lifetime analysis conducted in this paper.

5.1. Forced-Water Cooling

For the forced-water cooling system, IGBT modules are mounted on a water cooled heat sink. The water is circulated in and out of the heat sink using a pump, as shown in Figure 3. Two different configurations of the forced cooling system were evaluated in this paper:

- Six-pass system;
- Four-pass system.

Two different forced-water cooling systems are evaluated to demonstrate that further improvement in lifetime is possible by overrating the heat sink. There is also a possibility of overrating a heat sink by increasing the flow rate of the coolant. However, the latter is not investigated here.

In the 6-pass system, three modules (each corresponding to one phase of the generator side converter) are mounted on a single heat sink. This is shown in Figure 12. In the 4-pass system, only one phase module is mounted on a single heat sink. The necessary thermal parameters corresponding to each of these cooling configurations are listed in Table 4. The heat sinks correspond to the commercial manufacturer Wakefield-Vette [57].

Figure 13 shows the thermal circuit for the IGBT module coupled with the water cooled heat sink. The combined Cauer–Foster network used in Figure 13 is based on [5,58]. For simplification, uniform heat sink temperatures are assumed for all the modules (IGBTs as well as diodes) mounted on the same heat sink [45].

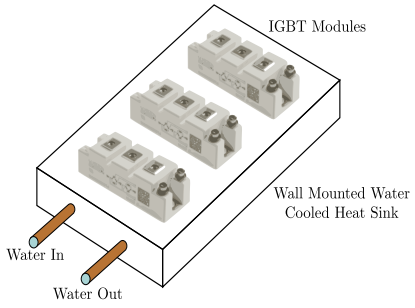

Figure 12. Three phase modules of the generator side converter mounted on a single water cooled heat sink (6-pass cold plate from Wakefield-Vette). In the case of 4-pass cold plate, only one phase module is mounted on each cold plate.

Table 4. Forced-water cooling parameters.

Parameter	Value
6-pass cold plate	
No. of dual IGBT modules per heat sink	3
Rated fluid flow rate	5 L/min
Fluid inlet temperature	15 °C
Thermal resistance $R_{th,c-a}$	0.01 K/W
Thermal capacitance	1930 W.s/K
Cold plate dimensions	0.304 m × 0.177 m × 0.0152 m
4-pass cold plate	
No. of dual IGBT modules per heat sink	1
Rated fluid flow rate	5 L/min
Fluid inlet temperature	15 °C
Thermal resistance $R_{th,c-a}$	0.02 K/W
Thermal capacitance	690 W.s/K
Cold plate dimensions	0.152 m × 0.127 m × 0.0152 m

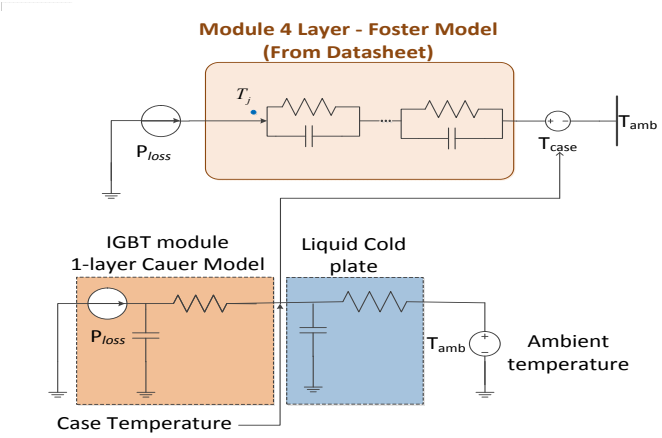

Figure 13. Thermal circuit for determining IGBT and diode junction temperatures in an actively cooled converter, adapted from [5]. T_j, shown in the figure, is the junction temperature of interest in the lifetime model used in this paper. This T_j can correspond to either the junction temperature of the IGBT or the diode, depending on which 4-layer Foster network is used.

5.2. Passively Cooled System

Figure 14 shows the placement of the switches in the passively cooled converter. Each module corresponds to a phase leg of the generator side converter and is mounted on a separate mounting plate. The mounting plate is made of a thermally conductive material, such as copper [5]. The dimensions of the mounting plate are listed in Table 5. For sake of brevity, the detailed modelling of the passive cooling system is omitted here. The system used here is the same as in [2], and the modelling of the passively cooled system can be found in the same paper.

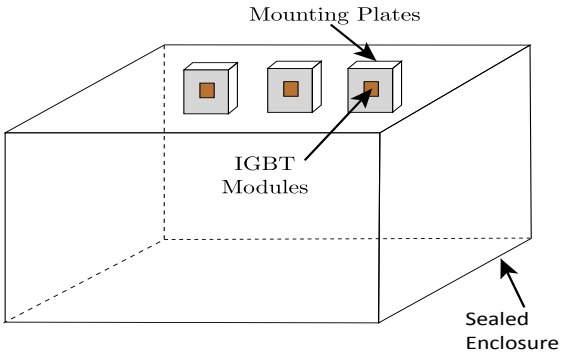

Figure 14. Three phase IGBT modules for generator side converter mounted on the inner walls of the submerged cabinet via a copper mounting plate. The copper mounting plate minimizes the spreading thermal resistance [5].

There is an important point of difference between the active and the passive cooling systems. Whereas in the active cooling system, R_{s-a} (sink-to-ambient thermal resistance) is assumed to be constant, the same cannot be done in the passively cooled system. The reason is that the external convective heat transfer coefficient in Figure 15 is a function of the heat flux from the IGBT power module [5,59]. As a result, the spreading thermal resistances in the enclosure frame and the mounting plate are modelled as variable resistances in Figure 15 [5,60].

Table 5. Passive water cooling parameters.

Parameter	Value
Enclosure wall thickness	0.010 m
Enclosure height	1.5 m
Enclosure width	0.5 m
Enclosure length	1.5 m
Cu mounting plate dimensions	0.171 m × 0.330 m
Cu mounting plate thickness	0.020 m
Thermal resistance $R_{th,c-a}$ (function of heat loss) including thermal paste	0.05–0.13 K/W [2]
Thermal capacitance	7862 W·s/K

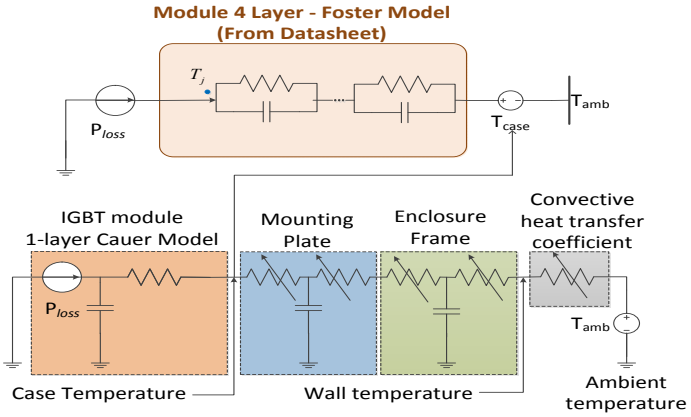

Figure 15. Thermal circuit for determining IGBT and diode junction temperatures in a passively cooled converter, from [5]. T_j, shown in the figure, is the junction temperature of interest in the lifetime model used in this paper. This T_j can correspond to either the junction temperature of the IGBT or the diode, depending on which 4-layer Foster network is used.

6. Case Study: Lifetime Analysis of 110 kW Tidal Turbines

In this section, the cooling systems in the submerged power converter for a 110 kW tidal turbine described in Section 3 are compared. The analysis is divided into two parts. Section 6.1 compares different cooling systems in terms of mean junction temperatures, temperature cycling amplitudes, lifetime of the IGBT modules, and annual losses in the IGBT modules for the active stall-controlled tidal turbine. On the other hand, Section 6.2 compares IGBT lifetimes in pitch-controlled and active stall-controlled turbines. In both cases, the lifetime of the IGBT modules is taken to be the lifetime of the diodes in the generator side converter. This is because the lifetime of the diodes on the generator side converter is the minimum of all IGBTs and diodes in the back-to-back converter shown in Figure 7 [2].

6.1. Comparison of Different Cooling Systems

Figure 16 demonstrates the speed variation of the generator as a consequence of the variation in the tidal stream velocity for the active speed stall-controlled turbine. The tidal velocity variations correspond to a part of Figure 4. Because the velocity at all times in Figure 16 is greater than the rated speed of 2.5 m/s, the generator power is maintained at 110 kW. Consequently, the rise/fall in the generator speed is reflected by corresponding fall/rise in the rms value of the generator phase currents, as seen in Figure 17.

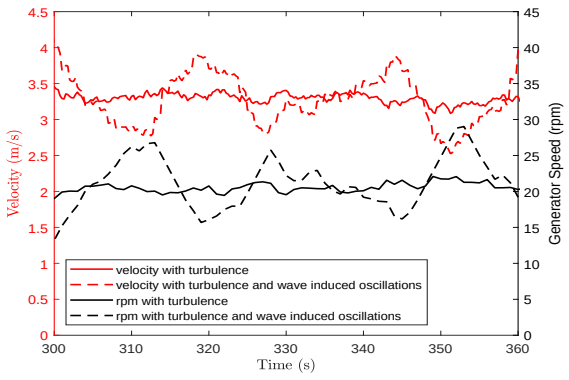

Figure 16. Active speed stall control of generator speed as a function of change in tidal stream velocity. Mean tidal velocity in this image is set at 3.3 m/s [2].

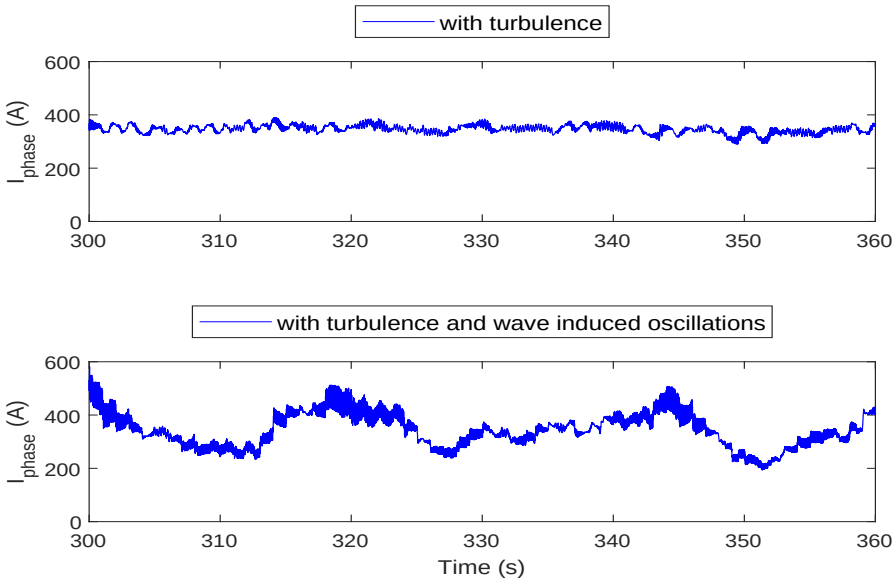

Figure 17. Generator phase currents (rms values). The variations in the phase current value are a direct consequence of the generator speed variations in Figure 16. This also illustrates why an IGBT module with 600 A rating was selected in this paper. The above graph would have depicted a flat line (about 380 A) without any velocity oscillations.

Figure 18 shows the estimated lifetime for the IGBT modules including the effects of turbulence, with and without the impact of surface waves. Clearly, forced-water cooling systems show significantly improved lifetime values over passive cooling systems. However, this increase in lifetime reduces when waves are also considered, in addition to turbulence.

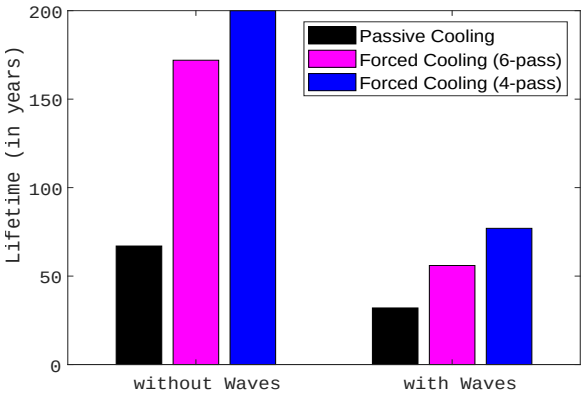

Figure 18. Estimated lifetime of the IGBT modules on the generator side converter with different cooling systems.

Even though there seems to be a significant difference in lifetime, the annual IGBT module losses in the generator side converter do not seem to be that different. This can be seen in Table 6. The losses in the passive cooling system are higher because higher junction temperatures also mean more losses in the IGBT modules. Figure 19 shows the mean junction temperatures as a function of tidal stream velocity. The passive cooling system has higher thermal resistance (sink-to-ambient) compared to forced-water cooling systems. Therefore, similar magnitudes of losses result in a higher temperature compared to the forced-water cooling systems.

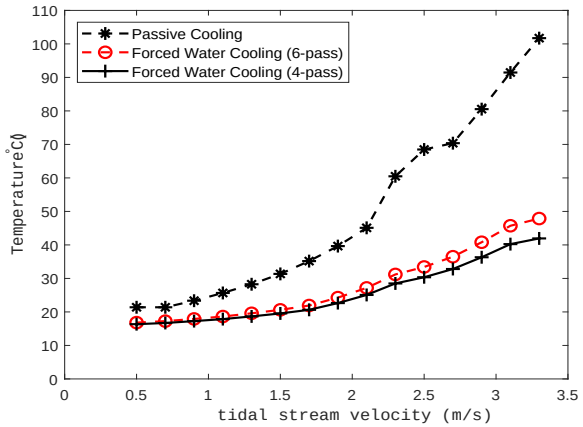

Figure 19. Comparison of mean junction temperatures between different cooling systems as a function of tidal stream velocity. Data for passive cooling is taken from mbox[2].

Table 6. Annual loss in the generator side converter for passive and active cooling systems, without waves.

Cooling System	IGBTs Loss (in MWh)	Diodes Loss (in MWh)
Passive cooling	2.11	2.53
Forced-water cooling (6-pass cold plate)	1.90	2.36
Forced-water cooling (4-pass cold plate)	1.89	2.35

There is not much difference between the mean temperatures of 4-pass and 6-pass cooling systems, except at higher tidal velocities. The difference in lifetimes of 6-pass and 4-pass cooling systems is because bulk lifetime consumption also occurs at higher tidal velocities. This is shown in Figure 20. This predominant lifetime consumption at high velocities is a consequence of the active stall control mechanism. In the active control strategy, at higher tidal velocities, rated power is delivered at a lower rpm and higher currents. This means more losses in the IGBT modules and hence more lifetime consumption. In other words, lifetime consumption below rated tidal speed can be neglected.

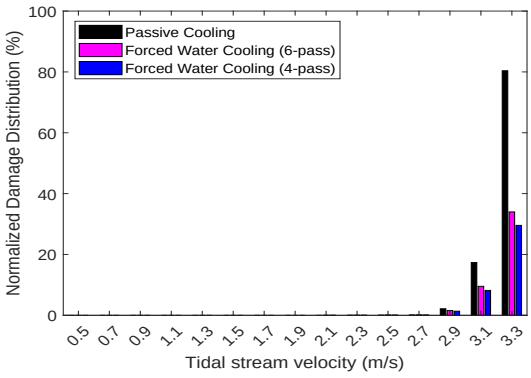

Figure 20. Annual damage distribution between different cooling systems as a function of tidal stream velocity. The values are normalized with respect to annual damage in passively cooled systems. Lifetime consumption mostly happens at higher tidal velocities.

Figures 21 and 22 show the diode junction temperature variation corresponding to the velocity variations in Figure 16. The amplitude of thermal cycling appears similar in all the three cases. Although passive systems have a higher thermal time constant for the heat sink, for cycling of the junction temperature, IGBT/diode thermal capacitances are more influential.

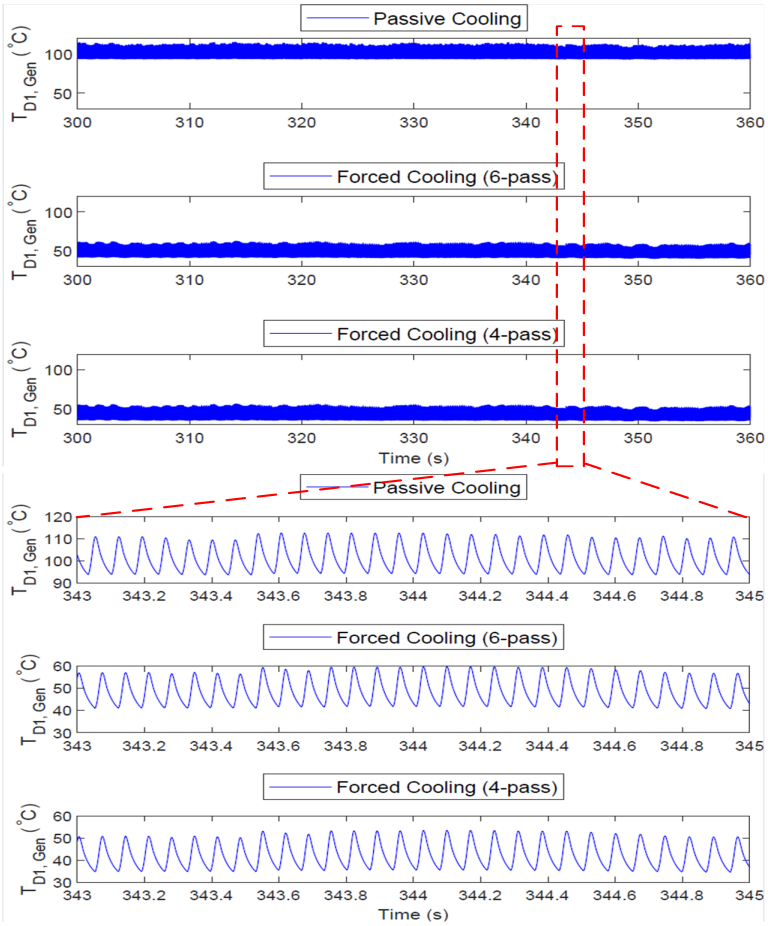

Figure 21. Comparison of cooling systems in terms of diode junction temperature cycling considering only turbulence in tidal stream velocity shown in Figure 16. This plot only corresponds to a time duration of 60 s under certain turbulence conditions. Results at different time instants and different values of mean tidal velocity and turbulence will give different values.

From the above discussion, we conclude that the difference in the lifetime for different cooling systems is primarily due to the difference in mean junction temperatures, and not so much due to thermal cycling. This is shown more clearly in Figure 23. On the other hand, considering the same cooling system, the lifetime reduction when including waves is due to the higher amplitude of thermal cycling.

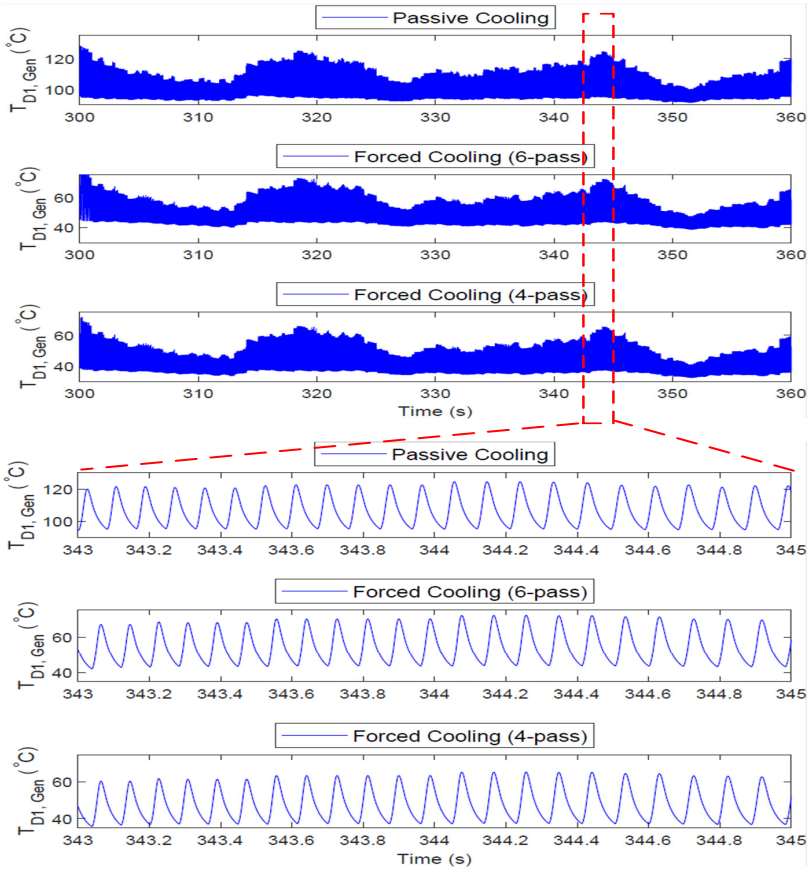

Figure 22. Comparison of cooling systems in terms of diode junction temperature cycling considering both turbulence and waves in tidal stream velocity shown in Figure 16.

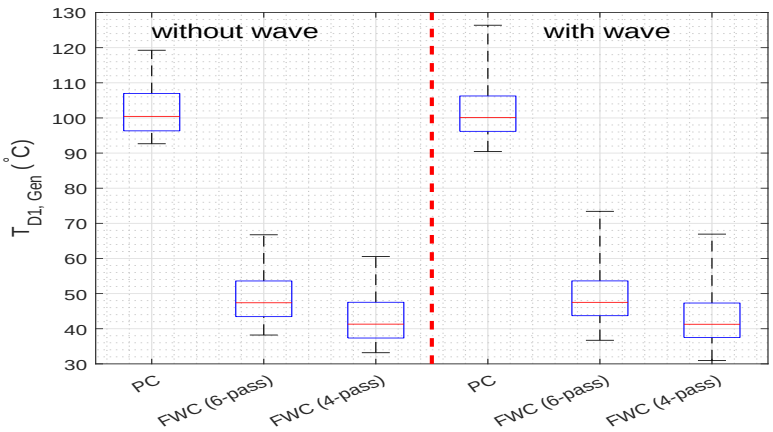

Figure 23. Diode junction temperature swing for different cooling systems at mean velocity of 3.3 m/s and TI value of 13%. Temperature swing is shown without waves and with a wave of H_s = 5.75 m and T_p = 11 s. For different cooling systems with same wave conditions, the temperature swing is nearly the same, albeit with a difference in mean temperatures. However, for the same cooling system, with and without waves, the mean temperature is the same but with a difference in temperature swing. PC—passive cooling; FWC—forced-water cooling.

6.2. Comparing Active Speed Stall and Pitch Control

Here, the comparison of the lifetime of IGBT modules in active stall- and pitch-controlled turbines is given. This analysis has only been done considering the forced-water cooling (6-pass coldplate) system. Table 7 shows the lifetime values for pitch and active

stall turbines. Lifetime values of pitch-controlled turbines are large because the device (IGBT) selection was done considering the active stall control (i.e., at high rms current values). The main reason for this is the lower mean junction temperature and temperature cycling experienced in pitch-controlled turbines, especially at higher tidal velocities, see Figure 24. Because the IGBT was overrated for the pitch-controlled turbine, it can be said that overrating the IGBT also improves the lifetime.

Table 7. IGBT lifetime comparison between active speed stall-controlled and pitch-controlled turbines.

Turbine	Lifetime (in Years)
Active speed stall control	55
Pitch control	30×10^3

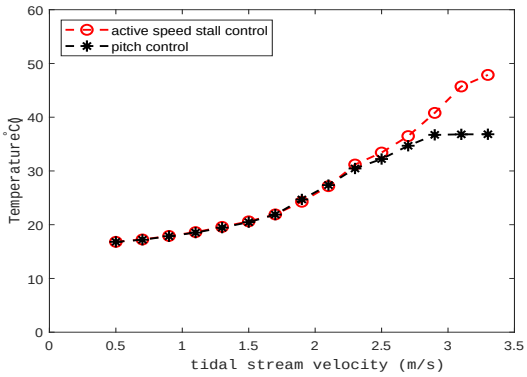

Figure 24. Mean junction temperatures of the diode (in the generator side converter) as a function of tidal stream velocity. Both turbines deliver the same power, albeit at different generator speeds. Below 2.5 m/s, active stall-controlled turbine operates at higher speed and thus has a lower temperature. Above 2.5 m/s, pitch-controlled turbine runs at higher speed. See Figure 6.

For the similar power rating and turbine size, pitch-controlled turbines draw a lower phase current above the rated speed because of smaller oscillations and a higher mean value of generator speed (see Figures 25 and 26). Consequently, the diode junction temperature has a lower mean value and lower amplitude of temperature cycling, as seen in Figure 27. Another point to note is the distribution of the lifetime damage with respect to the tidal stream velocity in active speed stall and pitch-controlled turbines, as shown in Figure 28.

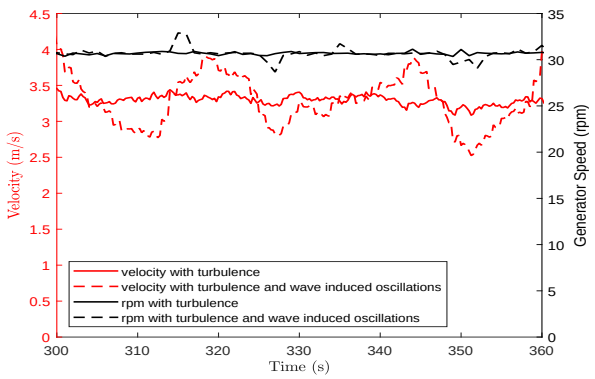

Figure 25. Variation of generator speed as a function of change in tidal stream velocity in a pitch-controlled turbine. Compare this with the generator speed variations in Figure 16.

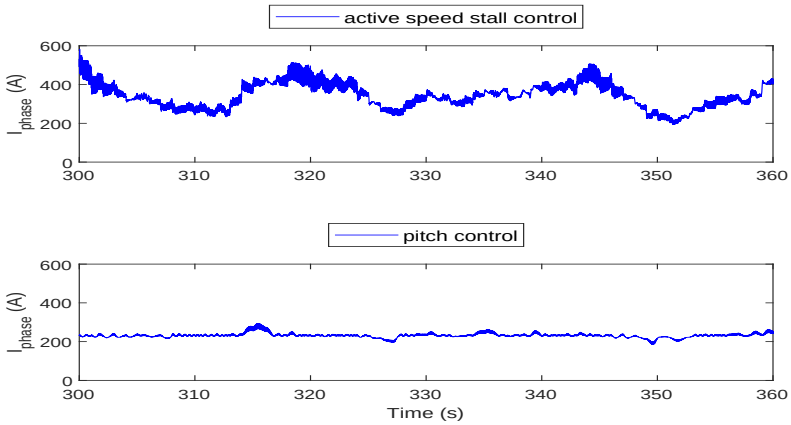

Figure 26. Generator phase currents (rms values) in the active speed stall- and the pitch-controlled turbine, under the influence of turbulence and wave-induced tidal stream velocity oscillation (as shown in Figure 4).

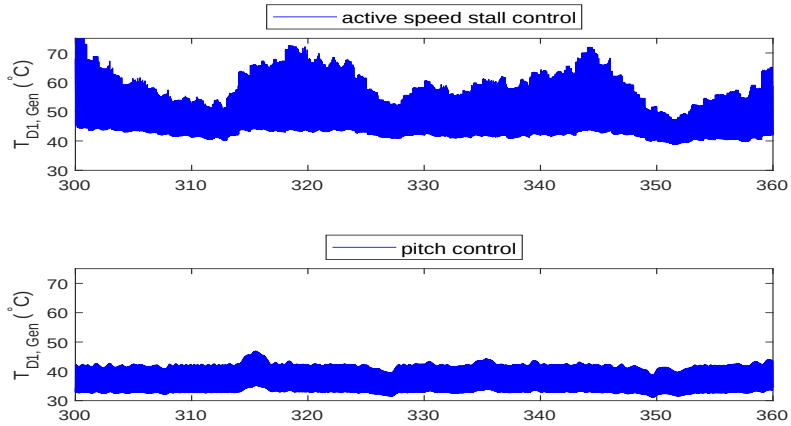

Figure 27. Comparison of the diode junction temperatures in turbines with active stall control and pitch control. It is clearly seen that pitch control mitigates the diode temperature cycling by maintaining nearly the same current even under significant wave-induced oscillations by virtue of maintaining nearly the same generator speed.

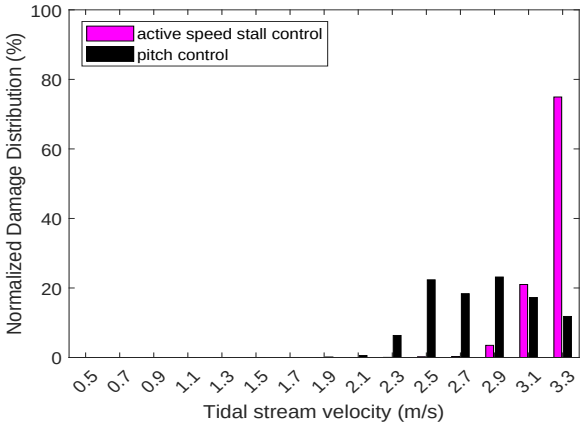

Figure 28. Damage distribution in active stall-controlled and pitch-controlled turbines (each normalized to 100%). Overall IGBT lifetime in the pitch-controlled turbine is much higher than in the active stall-controlled turbine. Whereas the lifetime consumption is concentrated at higher tidal velocities in the active stall-controlled turbine, it is more distributed in the pitch-controlled turbine.

7. Conclusions

In this paper, active and passive cooling systems for TST converters were compared based on the useful lifetime. The cooling systems were compared for the active stall-controlled as well as pitch-controlled tidal turbines. The comparison assumed thermal cycling as the main failure mode in IGBT modules. The results indicate that the forced-water cooling (active) system can yield a significant improvement in the lifetime of IGBT modules over passive systems; this result is valid for stall-controlled as well as pitch-controlled turbines. This improvement is primarily due to the decrease in the mean junction temperature of the IGBT modules rather than the decrease in the amplitude of thermal cycling. In other words, the amplitude of the thermal cycling is determined by the IGBT thermal capacitance (junction-to-case) and not the capacitance of the cooling system. When comparing the stall-controlled and pitch-controlled turbines, it was observed that the lifetime of the IGBT modules increases significantly when pitch control is used instead of the active stall control. Furthermore, in the pitch-controlled turbine, lifetime damage is more widespread over the tidal velocity range rather than just being concentrated at higher tidal velocities, as is the case in the active stall-controlled turbine. These conclusions hold true irrespective of the type of cooling system used in the converter.

Compared to the active cooling system, the passive cooling system is inherently more reliable, but it results in a lower estimated lifetime of IGBT modules. However, through this work, it is shown that passive cooling systems can still achieve acceptable lifetimes in TST converters and hence must be considered in future TST systems to lower the cost of levelized energy.

In the future, for a better understanding of the performance of cooling systems, it is important that the effect of natural processes, such as biofouling on the converter cabinet surface, is also investigated. This study neglected any deterioration in the cooling efficiency of the system over time due to biofouling. A way forward could be to estimate a reliable safety factor to account for the effects of biofouling, as such processes are generally difficult to model and heavily dependent on site conditions.

Author Contributions: Conceptualization, F.W.; Data curation, F.W.; Formal analysis, F.W.; Funding acquisition, H.P.; Investigation, F.W.; Methodology, F.W. and U.S.; Project administration, H.P.; Software, F.W. and U.S.; Supervision, J.D. and H.P.; Validation, J.D. and H.P.; Writing—original draft, F.W.; Writing—review and editing, F.W., U.S., J.D. and H.P. All authors have read and agreed to the published version of the manuscript.

Funding: The authors have been supported by the TiPA project (Tidal turbine Power take-off Accelerator), which has received funding from the European Union's Horizon 2020 research and innovation programme under grant agreement No 727793, managed by the Innovation and Networks Executive Agency. This paper reflects only the authors' views; the Agency is not responsible for any use that may be made of the information the paper contains.

Institutional Review Board Statement: Not applicable.

Informed Consent Statement: Not applicable.

Data Availability Statement: Models used in this study can be found on https://data.4tu.nl/info/en/.

Acknowledgments: The authors would like to Antonio Jarquin-Laguna and George Lavidas for their help in securing necessary data for this study.

Conflicts of Interest: The authors declare no conflict of interest.

Appendix A

Appendix A.1. Mean Tidal Velocity

A typical tidal site with the frequency of occurrence as a function of tidal stream velocity is shown in Figure A1 [2].

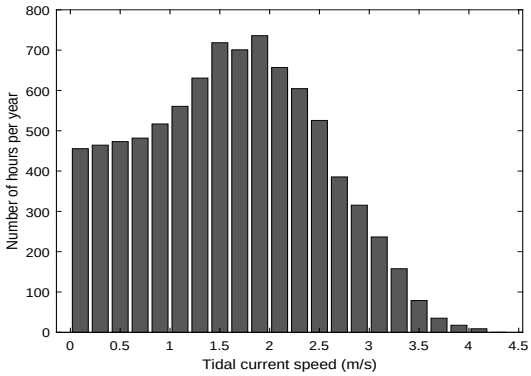

Figure A1. Tidal velocity distribution at EMEC site, Orkney [61].

Appendix A.2. Turbulence in the Sea

Different values of turbulence intensity (TI) are used for flood and ebb tides [2,62]. Table A1 lists TI values used in this paper. Please note that this analysis only uses the average value of TI; in reality, different values of TI are possible for the same mean tidal velocity.

Table A1. TI values used to generate time series of tidal stream velocity [2].

Mean Velocity Range (m/s)	Mean TI Values (%)
Ebb tide	
$0.5 \leq \bar{u} \leq 1.1$	13.9
$1.3 \leq \bar{u} \leq 3.3$	11.7
Flood tide	
$0.5 \leq \bar{u} \leq 1.1$	14.5
$1.3 \leq \bar{u} \leq 3.3$	12.0

Appendix A.3. Surface Waves

The surface wave conditions used in this analysis are listed in Tables A2 and A3, with their probability densities [2]. JONSWAP spectrum is chosen for the surface waves, in accordance with [2,63], with a peak enhancement factor, γ = 3.3 [2,34].

The probabilities are given to ensure all waves are included in proportion to their occurrence; neglecting this could result in grossly miscalculated lifetime values. In addition, because different wave conditions occur in summer and winter, two probability density tables, each corresponding to a representative summer (May) and winter month (Nov), were used in this study [64].

Table A2. Probability density (%) of waves according to significant wave heights (Hs) and peak time periods (Tp) for May 2009 at Orkney [2].

Tp (s), Hs (m)	0.25	0.75	1.25	1.75	2.25	2.75	3.25	3.75	4.25	4.75	5.25	5.75	6.25
3	6.92	2.82	2.35	0	0	0	0	0	0	0	0	0	0
5	4.97	0.27	0.87	0.47	0	0	0	0	0	0	0	0	0
7	3.96	0	0.07	1.75	1.01	0	0.74	0	0	0	0	0	0
9	5.98	0	1.81	0.34	0.2	0	0.94	0.87	0.40	0	0	0	0
11	2.48	3.76	4.77	6.72	6.18	3.96	2.08	0.07	1.61	0.27	0.27	0.13	0
13	0.47	1.07	2.89	4.91	2.22	2.01	4.57	4.30	0.27	0	0	0.13	0.20
15	0.47	0.67	0.13	0.34	0	0.20	0.13	2.55	0.87	0.40	0.20	0.34	0
17	0	0	0	0	0	0	0.13	0.26	1.14	0	0	0	0

Table A3. Probability density (%) of waves according to significant wave heights (Hs) and peak time periods (Tp) for November 2009 at Orkney [2].

Tp (s), Hs (m)	0.25	0.75	1.25	1.75	2.25	2.75	3.25	3.75	4.25	4.75	5.25	5.75	6.25
3	0	0.27	2.22	0	0	0	0	0	0	0	0	0	0
5	0	0.69	6.11	1.04	1.32	0.07	0	0	0	0	0	0	0
7	0	0	0.55	1.25	1.87	3.61	2.22	0.42	0	0	0	0	0
9	0	0	0.83	0	0.35	0.76	1.53	1.11	0	0	0	0	0
11	0	2.64	3.40	7.22	7.29	0.35	0	0	0	0	0	0	0
13	0	2.15	2.29	4.30	13.95	10.07	2.78	0.69	0	0	0	0	0
15	0	0	1.46	0.63	1.18	7.5	1.87	1.39	0	0	0	0	0
17	0	0	0.21	0	0	0.35	2.01	0	0	0	0	0	0

References

1. Magagna, D.; Monfardini, R.; Uihlein, A. *JRC Ocean Energy Status Report*; Publications Office of the European Union: Luxembourg, 2016. Available online: https://setis.ec.europa.eu/sites/default/files/reports/ocean_energy_report_2016.pdf (accessed on 1 June 2020)
2. Wani, F.; Shipurkar, U.; Dong, J.; Polinder, H.; Jarquin-Laguna, A.; Mostafa, K.; Lavidas, G. Lifetime analysis of IGBT power modules in passively cooled tidal turbine converters. *Energies* **2020**, *13*, 1875. [CrossRef]
3. Qian, C.; Gheitaghy, A.; Fan, J.; Tang, H.; Sun, B.; Ye, H.; Zhang, G. Thermal management on IGBT power electronic devices and modules. *IEEE Access* **2018**, *6*, 12868–12884. [CrossRef]
4. Wintrich, A.; Nicolai, U.; Tursky, W.; Reimann, T. *Application Manual Power Semiconductors*; SEMIKRON International GmbH: Nuremberg, Germany, 2015. Available online: https://www.semikron.com/dl/service-support/downloads/download/semikron-application-manual-power-semiconductors-english-en-2015/ (accessed on 10 January 2020).
5. Wani, F.; Shipurkar, U.; Dong, J.; Polinder, H. A study on passive cooling in subsea power electronics. *IEEE Access* **2018**, *6*, 67543–67554. [CrossRef]
6. Toma, D.; Mànuel-Làzaro, A.; Nogueras, M.; Del Rio, J. Study on heat dissipation and cooling optimization of the junction box of OBSEA seafloor observatory. *IEEE/ASME Trans. Mechatron.* **2014**, *20*, 1301–1309. [CrossRef]
7. Whitby, B.; Ugalde-Loo, C. Performance of pitch and stall regulated tidal stream turbines. *IEEE Trans. Sustain. Energy* **2014**, *5*, 64–72. [CrossRef]
8. Polinder, H.; Bang, D.; Van Rooij, R.P.; McDonald, A.S.; Mueller, M. 10 MW wind turbine direct-drive generator design with pitch or active speed stall control. In Proceedings of the IEEE International Electric Machines and Drives Conference, Antalya, Turkey, 3–5 May 2007; pp. 1390–1395
9. Wani, F.; Polinder, H. A Review of Tidal Current Turbine Technology: Present and Future. In Proceedings of the 12th European Wave and Tidal Energy Conference (EWTEC 2017), Cork, Ireland, 27 August–1 September 2017.
10. Carroll, J.; McDonald, A.; McMillan, D. Reliability comparison of wind turbines with DFIG and PMG drive trains. *IEEE Trans. Energy Convers.* **2015**, *30*, 663–670. [CrossRef]
11. Spinato, F.; Tavner, P.; van Bussel, G.; Koutoulakos, E. Reliability of wind turbine subassemblies. *IET Renew. Power Gener.* **2009**, *3*, 387–401. [CrossRef]
12. CATAPULT. Portfolio Review 2016: System Performance, Availability and Reliability Trends Analysis (SPARTA). 2016. Available online: https://s3-eu-west-1.amazonaws.com/media.ore.catapult/wp-content/uploads/2017/03/28102600/SPARTAbrochure_20March-1.pdf (accessed on 15 April 2020)
13. Yang, S.; Xiang, D.; Bryant, A.; Mawby, P.; Ran, L.; Tavner, P. Condition monitoring for device reliability in power electronic converters: A review. *IEEE Trans. Power Electron.* **2010**, *25*, 2734–2752. [CrossRef]
14. Fischer, K.; Pelka, K.; Puls, S.; Poech, M.; Mertens, A.; Bartschat, A.; Tegtmeier, B.; Broer, C.; Wenske, J. Exploring the causes of power-converter failure in wind turbines based on comprehensive field-data and damage analysis. *Energies* **2019**, *12*, 593. [CrossRef]
15. Shipurkar, U.; Lyrakis, E.; Ma, K.; Polinder, H.; Ferreira, J. Lifetime comparison of power semiconductors in three-level converters for 10MW wind turbine systems. *IEEE J. Emerg. Sel. Top. Power Electron.* **2018**, *6*, 1366–1377. [CrossRef]
16. Choi, U.; Blaabjerg, F.; Iannuzzo, F.; Jørgensen, S. Junction temperature estimation method for a 600 V, 30 A IGBT module during converter operation. *Microelectron. Reliab.* **2015**, *15*, 2022–2026. [CrossRef]
17. Ma, K.; Blaabjerg, F.; Liserre, M. Thermal analysis of multilevel grid-side converters for 10-MW wind turbines under low-voltage ride through. *IEEE Trans. Ind. Appl.* **2013**, *49*, 909–921. [CrossRef]
18. Hu, Z.; Ge, X.; Xie, D.; Zhang, Y.; Yao, B.; Dai, J.; Yang, F. An aging-degree evaluation method for IGBT bond wire with online multivariate monitoring. *Energies* **2019**, *12*, 3962. [CrossRef]
19. Hu, Y.; Shi, P.; Li, H.; Yang, C. Health condition assessment of base-plate solder for multi-chip IGBT module in wind power converter. *IEEE Access* **2019**, *7*, 72134–72142. [CrossRef]

20. De Rijck, A.; Huisman, H. Power Semiconductor Device Adaptive Cooling Assembly. U.S. Patent 8,547,687, 2013. Available online: https://patentimages.storage.googleapis.com/cf/bf/f1/f8fd4113102d38/US8547687.pdf (accessed on 5 April 2020).
21. Shipurkar, U. Improving the Availability of Wind Turbine Generator Systems. Ph.D. Thesis, Delft University of Technology, Delft, The Netherlands, 2019.
22. Yerasimou, Y.; Pickert, V.; Ji, B.; Song, X. Liquid metal magnetohydrodynamic pump for junction temperature control of power modules. *IEEE Trans. Power Electron.* **2018**, *33*, 10583–10593. [CrossRef]
23. Choi, U.; Lee, J. Comparative evaluation of lifetime of three-level inverters in grid-connected photovoltaic systems. *Energies* **2020**, *13*, 1227. [CrossRef]
24. Rajashekara, K.; Krishnamoorthy, H.; Naik, B. Electrification of subsea systems: Requirements and challenges in power distribution and conversion. *CPSS Trans. Power Electron. Appl.* **2017**, *2*, 259–266. [CrossRef]
25. Andresen, M.; Ma, K.; Buticchi, G.; Falck, J.; Blaabjerg, F.; Liserre, M. Junction temperature control for more reliable power electronics. *IEEE Trans. Power Electron.* **2017**, *33*, 765–776. [CrossRef]
26. Chen, G.; Cai, X. Adaptive control strategy for improving the efficiency and reliability of parallel wind power converters by optimizing power allocation. *IEEE Access* **2018**, *6*, 6138–6148. [CrossRef]
27. Weckert, M.; Roth-Stielow, J. Chances and limits of a thermal control for a three-phase voltage source inverter in traction applications using permanent magnet synchronous or induction machines. In Proceedings of the 14th European Conference on Power Electronics and Applications, Birmingham, UK, 30 August–1 September 2011; IEEE: Piscataway, NJ, USA, 2011; pp. 1–10.
28. Ma, K.; Blaabjerg, F. Thermal optimised modulation methods of three-level neutral-point-clamped inverter for 10 mw wind turbines under low-voltage ride through. *IET Power Electron.* **2012**, *5*, 920–927. [CrossRef]
29. Andresen, M.; Kuprat, J.; Raveendran, V.; Falck, J.; Liserre, M. Active thermal control for delaying maintenance of power electronics converters. *Chin. J. Electr. Eng.* **2018**, *33*, 13–20.
30. Ma, K.; Liserre, M.; Blaabjerg, F. Reactive power influence on the thermal cycling of multi-mw wind power inverter. *IEEE Trans. Ind. Appl.* **2013**, *49*, 922–930. [CrossRef]
31. Wu, L.; Castellazzi, A. Temperature adaptive driving of power semiconductor devices. In Proceedings of the 2010 IEEE International Symposium on Industrial Electronics, Bari, Italy, 4–7 July 2010; pp. 1110–1114.
32. Ma, K.; Blaabjerg, F. The impact of power switching devices on the thermal performance of a 10 MW wind power NPC converter. *Energies* **2012**, *5*, 2559–2577. [CrossRef]
33. Yang, Y.; Wang, H.; Sangwongwanich, A.; Blaabjerg, F. Design for reliability of power electronic systems. In *Power Electronics Handbook*; Elsevier: Amsterdam, The Netherlands, 2018; pp. 1423–1440.
34. Chen, H.; Xie, W.; Chen, X.; Han, J.; Ait-Ahmed, N.; Zhou, Z.; Tang, T.; Benbouzid, M. Fractional-order PI control of dfig-based tidal stream turbine. *J. Mar. Sci. Eng.* **2020**, *8*, 309. [CrossRef]
35. Gu, Y.; Liu, H.; Li, W.; Lin, Y.; Li, Y. Integrated design and implementation of 120-kW horizontal-axis tidal current energy conversion system. *Ocean Eng.* **2017**, *37*, 684–703. [CrossRef]
36. Jahromi, M.; Maswood, A.; Tseng, K. Design and evaluation of a new converter control strategy for near-shore tidal turbines. *IEEE Trans. Ind. Electron.* **2012**, *60*, 5648–5659. [CrossRef]
37. Zhou, Z.; Scuiller, F.; Charpentier, J.F.; El, M.; Benbouzid, H.; Tang, T. Power control of a non-pitchable PMSG-based marine current turbine at overrated current speed with flux-weakening strategy. *IEEE J. Ocean. Eng.* **2015**, *40*, 536–545. [CrossRef]
38. Ma, K.; Liserre, M.; Blaabjerg, F.; Kerekes, T. Thermal loading and lifetime estimation for power device considering mission profiles in wind power converter. *IEEE Trans. Power Electron.* **2014**, *30*, 590–602. [CrossRef]
39. Givaki, K.; Parker, M.; Jamieson, P. Estimation of the power electronic converter lifetime in fully rated converter wind turbine for onshore and offshore wind farms. In Proceedings of the IET Power Electronics, Machines and Drives (PEMD 2014), Manchester, UK, 8–10 April 2014.
40. Denk, M.; Bakran, M. Comparison of counting algorithms and empiric lifetime models to analyze the load-profile of an IGBT power module in a hybrid car. In Proceedings of the IEEE 2013 3rd International Electric Drives Production Conference (EDPC), Nuremberg, Germany, 29–30 October 2013; pp. 1–6.
41. Wang, Y.; Jones, S.; Dai, A.; Liu, G. Reliability enhancement by integrated liquid cooling in power IGBT modules for hybrid and electric vehicles. *Microelectron. Reliab.* **2014**, *54*, 1911–1915. [CrossRef]
42. Thoben, M.; Sauerland, F.; Mainka, K.; Edenharter, S.; Beaurenaut, L. Lifetime modeling and simulation of power modules for hybrid electrical vehicles. *Microelectron. Reliab.* **2014**, *54*, 1806–1812. [CrossRef]
43. I. Technologies, IGBT Modules. Available online: https://www.infineon.com/cms/en/product/power/igbt/igbt-modules/ (accessed on 10 January 2020).
44. Zhou, Z.; Khanniche, M.; Igic, P.; Kong, S.; Towers, M.; Mawby, P. A fast power loss calculation method for long real time thermal simulation of IGBT modules for a three-phase inverter system. In Proceedings of the European Conference on Power Electronics and Applications, Dresden, Germany, 11–14 September 2005.
45. Lemmens, J.; Vanassche, P.; Driesen, J. Optimal control of traction motor drives under electrothermal constraints. *IEEE J. Emerg. Sel. Top. Power Electron.* **2014**, *2*, 249–263. [CrossRef]
46. Musallam, M.; Johnson, C.M. Real-time compact thermal models for health management of power electronics. *IEEE Trans. Power Electron.* **2010**, *25*, 1416–1425. [CrossRef]

47. Reichl, J.; Ortiz-Rodriguez, J.M.; Hefner, A.; Lai, J.S. 3D thermal component model for electrothermal analysis of multichip power modules with experimental validation. *IEEE Trans. Power Electron.* **2014**, *30*, 3300–3308. [CrossRef]
48. Riccio, M.; De Falco, G.; Maresca, L.; Breglio, G.; Napoli, E.; Irace, A.; Iwahashi, Y.; Spirito, P. 3d electro-thermal simulations of wide area power devices operating in avalanche condition. *Microelectron. Reliab.* **2012**, *52*, 2385–2390. [CrossRef]
49. Xu, S.Z.; Peng, Y.F.; Li, S.Y. Application thermal research of forced-air cooling system in high-power NPC three-level inverter based on power module block. *Case Stud. Therm. Eng.* **2016**, *8*, 387–397. [CrossRef]
50. Yun, C.S.; Malberti, P.; Ciappa, M.; Fichtner, W. Thermal component model for electrothermal analysis of igbt module systems. *IEEE Trans. Adv. Packag.* **2001**, *24*, 401–406.
51. Ma, K. Electro-thermal model of power semiconductors dedicated for both case and junction temperature estimation. In *Power Electronics for the Next Generation Wind Turbine System*; Springer: Berlin/Heidelberg, Germany, 2015; pp. 139–143.
52. Luo, Z.; Ahn, H.; Nokali, M. A thermal model for insulated gate bipolar transistor module. *IEEE Trans. Power Electron.* **2004**, *19*, 902–907. [CrossRef]
53. Bahman, A.; Ma, K.; Blaabjerg, F. Thermal impedance model of high power IGBT modules considering heat coupling effects. In Proceedings of the International Power Electronics and Application Conference and Exposition, Shanghai, China, 5–8 November 2014; pp. 1382–1387.
54. Bayerer, R.; Herrmann, T.; Licht, T.; Lutz, J.; Feller, M. Model for power cycling lifetime of IGBT modules—Various factors influencing lifetime. In Proceeding of the 5th International Conference on Integrated Power Systems (CIPS), Nuremberg, Germany, 11–13 March 2008; pp. 1–6.
55. Climate-data.org.Climate: Kirkwall. Available online: https://en.climate-data.org/location/56552/ (accessed on 5 October 2019).
56. Wu, R.; Wang, H.; Pedersen, K.; Ma, K.; Ghimire, P.; Iannuzzo, F.; Blaabjerg, F. A Temperature-Dependent Thermal Model of IGBT Modules Suitable for Circuit-Level Simulations. *IEEE Trans. Ind. Appl.* **2016**, *52*, 3306–3314. [CrossRef]
57. Wakefield-Vette. Exposed Tube Liquid Cold Plates. *Tech. Rep.* **2016**. Available online: https://eu.mouser.com/datasheet/2/433/Wakefield-Vette_Exposed_Tube_Liquid_Cold_Plates_Fi-1500597.pdf (accessed on 25 March 2020).
58. Ma, K.; Yang, Y.; Blaabjerg, F. Transient modelling of loss and thermal dynamics in power semiconductor devices. In Proceedings of the Energy Conversion Congress and Exposition (ECCE), Pittsburg, PA, USA, 14–18 September 2014; pp. 5495–5501.
59. Cengel, Y.A.; Ghajar, J. *Heat and Mass Transfer, Fundamentals & Application, Fifth Edition in SI Units*; McGraw-Hill: New York, NY, USA, 2014.
60. Muzychka, Y.; Culham, J.; Yovanovich, M. Thermal spreading resistance of eccentric heat sources on rectangular flux channels. *J. Electron. Packag.* **2003**, *125*, 178–185. [CrossRef]
61. CATAPULT. ReDAPT—Public Domain Report: Final (MC7.3). Technical Report. 2015. Available online: http://redapt.eng.ed.ac.uk/library/eti/reports/MC7.3%20Operations%20Final%20Report.pdf (accessed on 1 April 2020).
62. Sellar, B.; Wakelam, G.; Sutherland, D.; Ingram, D.; Venugopal, V. Characterisation of tidal flows at the european marine energy centre in the absence of ocean waves. *Energies* **2018**, *11*, 176. [CrossRef]
63. Zhou, Z.; Scuiller, F.; Charpentier, J.F.; Benbouzid, M.; Tang, T. Power smoothing control in a grid-connected marine current turbine system for compensating swell effect. *IEEE Trans. Sustain. Energy* **2013**, *4*, 816–826. [CrossRef]
64. Lavidas, G.; Venkatesan, V. Characterising the wave power potential of the scottish coastal environment. *Int. J. Sustain. Energy* **2017**, *37*, 684–703. [CrossRef]